Anal. Chem. **2007,** *79,* 4031−4039

Numerical Fluorescence Correlation Spectroscopy for the Analysis of Molecular Dynamics under Nonstandard Conditions

Michael J. Culbertson,† Joshua T. B. Williams,† Wayland W. L. Cheng,† Dee Ann Stults,† Emily R. Wiebracht,† John J. Kasianowicz,‡ and Daniel L. Burden*,†

Chemistry Department, Wheaton College, Wheaton, Illinois 60187, and EEEL Division, National Institute of Standards and Technology, Gaithersburg, Maryland 20899

The suitability of mathematical models used to extract kinetic information from correlated data constitutes a significant issue in fluorescence correlation spectroscopy (FCS). Standard FCS equations are derived from a simple Gaussian approximation of the optical detection volume, but some investigations have suggested this traditional practice can lead to inaccurate and misleading conclusions under many experimental circumstances, particularly those encountered in one-photon confocal measurements. Furthermore, analytical models cannot be derived for all measurement scenarios. We describe a novel numerical approach to FCS that circumvents conventional analytical models, enabling meaningful analyses even under extraordinarily unusual measurement conditions. Numerical fluorescence correlation spectroscopy (NFCS) involves quantitatively matching experimental correlation curves with synthetic curves generated via diffusion simulation or direct calculation based on an experimentally determined 3D map of the detection volume. Model parameters are adjusted iteratively to minimize the residual differences between synthetic and experimental correlation curves. In order to reduce analysis time, we distribute calculations across a network of processors. As an example of this new approach, we demonstrate that synthetic autocorrelation curves correspond well with experimental data and that NFCS diffusion measurements of Rhodamine B remain constant, regardless of the distortion present in a confocal detection volume.

Since its inception more than three decades ago,[1] fluorescence correlation spectroscopy (FCS) has become a widely used method for characterizing reaction dynamics, photophysical kinetics, molecular aggregation, conformational fluctuations, and translational motion in many chemical systems.[2] FCS has been widely applied to study materials as diverse as proteins,[3] DNA,[4] polyelectolytes,[5,6] colloids and nanoparticles,[7,8] organic thin films,[9−11] lubricants,[12] emulsions,[13] lipid membranes,[14] ionic liquids,[15] and infectious agents.[16] It has also been applied as a tool for measuring flow rates in microfluidic devices[17,18] and has been employed in the complex environment of living tissues and cells.[19]

In a typical one-photon FCS measurement,[20] a focused laser beam is directed into a fluid sample doped with a fluorescent tracer. As fluorescent particles diffuse in and out of the laser beam, the microscope objective collects a fraction of the fluorescence emission and transmits the collected light through a pinhole to a photodetector. The autocorrelation function of the time-domain fluorescence intensity fluctuation is then calculated:

$$G(\tau) = \frac{\langle I(t+\tau)I(t)\rangle}{\langle I(t)\rangle^2} \qquad (1)$$

where $I(t)$ is the real-time detected intensity, τ is a delay variable, t is time, and $< >$ indicates time averaging. The autocorrelated

* Corresponding author. E-mail: daniel.l.burden@wheaton.edu.
† Wheaton College.
‡ National Institute of Standards and Technology.

(1) Magde, D.; Elson, E. L.; Webb, W. W. *Biopolymers* **1974**, *13*, 29−61.
(2) Elson, E. L. *J. Biomed. Opt.* **2004**, *9*, 857−864.
(3) Chen, Y.; Muller, J. D.; Tetin, S. Y.; Tyner, J. D.; Gratton, E. *Biophys. J.* **2000**, *79*, 1074−1084.
(4) Tatarkova, S. A.; Berk, D. A. *Phys. Rev. E* **2005**, *71*, 41913.
(5) Pristinski, D.; Kozlovskaya, V.; Sukhishvili, S. A. *J. Chem. Phys.* **2005**, *122*, 14907.
(6) Van Rompaey, E.; Engelborghs, Y.; Sanders, N.; De Smedt, S. C.; Demeester, J. *Pharm. Res.* **2001**, *18*, 928−936.
(7) Lellig, C.; Wagner, J.; Hempelmann, R.; Keller, S.; Lumma, D.; Härtl, W. *J. Chem. Phys.* **2004**, *121*, 7022−7029.
(8) Weyermann, J.; Lochmann, D.; Georgens, C.; Rais, I.; Kreuter, J.; Karas, M.; Wolkenhauer, M.; Zimmer, A. *Eur. J. Pharm. Biopharm.* **2004**, *58*, 25−35.
(9) Czeslik, C.; Jansen, R.; Ballauff, M.; Wittemann, A.; Royer, C. A.; Gratton, E.; Hazlett, T. *Phys. Rev. E* **2004**, *69*, 21401.
(10) Casoli, A.; Schönhoff, M. *Biol. Chem.* **2001**, *382*, 363−369.
(11) Zhong, Z.; Lowry, M.; Wang, G.; Geng, L. *Anal. Chem.* **2005**, *77*, 2303−2310.
(12) Mukhopadhyay, A.; Bae, S. C.; Zhao, J.; Granick, S. *Phys. Rev. Lett.* **2004**, *93*, 236105.
(13) Burnett, G. R.; Rees, G. D.; Steytler, D. C.; Robinson, B. H. *Colloid Surf. A* **2004**, *250*, 171−178.
(14) Burns, A. R.; Frankel, D. J.; Buranda, T. *Biophys. J.* **2005**, *89*, 1081−1093.
(15) Werner, J. H.; Baker, S. N.; Baker, G. A. *Analyst* **2003**, *128*, 786−789.
(16) Schwille, P.; Bieschke, J.; Oehlenschlager, F. *Biophys. Chem.* **1997**, *66*, 211−228.
(17) Gösch, M.; Blom, H.; Holm, J.; Heino, T.; Rigler, R. *Anal. Chem.* **2000**, *72*, 3260−3265.
(18) Kuricheti, K. K.; Buschmann, V.; Weston, K. D. *Appl. Spectrosc.* **2004**, *58*, 1180−1186.
(19) Vukojević, V.; Pramanik, A.; Yakovleva, T.; Rigler, R.; Terenius, L.; Bakalkin, G. *Cell. Mol. Life Sci.* **2005**, *62*, 535−550.
(20) Thompson, N. L. In *Topics in fluorescence spectroscopy*; Lakowicz, J. R., Ed.; Plenum Press: New York, 1991; pp 337−378.

10.1021/ac062013m CCC: $37.00
Published on Web 04/21/2007

data are then fit with a mathematical model to obtain quantities of interest, such as the species' diffusion constant. Standard analytical expressions exist for two- and three-dimensional translation, triplet-state effects, reaction kinetics, particles in a bulk flow, and other measurement scenarios.[19] In addition, it is possible to derive expressions for more specialized situations, such as lateral diffusion with rare strong adsorption,[21] particles on buckled, undulating, or inclined membranes,[22] particles near fluctuating membranes,[23] or fluorescent tags embedded in polymer chains.[24]

These analytical fitting functions are typically derived using a 3D Gaussian approximation of the confocal detection volume:

$$P(r,z) = Ae^{-2r^2/\omega_1^2}e^{-2z^2/\omega_2^2} \qquad (2)$$

where P is the detection probability, A is a scaling factor, r and z are the radial and axial coordinates, and ω_1 and ω_2 are the $1/e^2$ widths characterizing the radial and axial dimensions. For simple open-volume diffusion measurements with a single diffusing species, the theoretical autocorrelation function derived for this profile is

$$G(\tau) = \frac{\gamma}{N}\left[1 + \frac{4D\tau}{\omega_1^2}\right]^{-1}\left[1 + \frac{4D\tau}{\omega_2^2}\right]^{-1/2} + 1 \qquad (3)$$

where D is the characteristic diffusion constant, N is the average number of molecules in the detection volume during the measurement, and γ is a shape factor equal to 0.3535 for idealized Gaussians. This spatial profile assumes that the characteristic radial width remains constant throughout the volume, producing an ellipsoidal geometry when multiplied by the axial term.

However, under commonly employed optical conditions, the radial width actually increases along the optical axis due to the contour of the focused laser beam (Figure 1A).[25−27] The actual shape of the detection volume results from the spatial overlap of the focused laser profile and the optical collection efficiency function, both of which depend on parameters such as the filling of the objective back aperture, the pinhole size, and the objective magnification. Polarization effects, refractive index mismatches, pinhole misalignment, cover slide thickness, and optical saturation also affect the size and shape of the detection volume.[28,29] Because not all of these factors can be characterized or corrected, differences between theory and experiment are guaranteed.[26,28,30,31] When standard analytic models are employed under nonideal circumstances, inaccuracies or misleading conclusions can result,

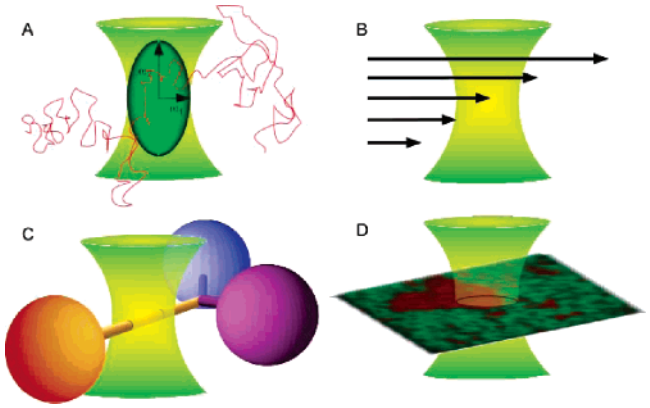

Figure 1. Example nonstandard measurement scenarios amenable to NFCS. (A) Analyses of molecular dynamics where the detection volume deviates from the idealized Gaussian geometry (characterized by ω_1 and ω_2). (B) Measurements of fluid velocity where a gradient flow profile exists within the detection volume. (C) Translational dynamics that are constrained to regions with subdetection volume dimensions, such as diffusion in or on a lipid nanotube. (D) Two-dimensional diffusion within a lipid membrane that contains microdomains or lipid rafts of differing local viscosity.

particularly if systematic residuals encourage the inappropriate application of highly parametrized models, such as those describing multiple diffusing species, anomalous diffusion, or transitions between bright and dark states. Some investigations indicate that diffusion results can be skewed by as much as 80% and that the axial ratio of the detection volume can easily diverge during calibration.[26]

Other nonstandard measurement scenarios impose altogether different spatial relationships and thus require more sophisticated models. For example, when measuring flow in pressurized microfluidic channels with dimensions similar to the detection volume, the FCS model needs to accommodate a gradient flow profile (Figure 1B). In other cases, nanoscale structures confine translation of fluorescent species to small regions within the detection volume (Figure 1C,D). Hac et al. found that the standard multicomponent FCS equations did not accurately describe the translational dynamics in multidomain two-component lipid membranes.[32] Other systems with nanoscale geometric constrains, such as polymeric cavities or nanotubular structures, present similar challenges to FCS analysis since fluorescent tracers cannot interact with the entire detection region in standard ways. But even for relatively simple constraints, such as diffusion in a linear nanotube[33] or translation in the presence of bias due to a laser gradient field,[34] the analytical derivation of an FCS model might not be possible. Given the increasing significance of nanoscale materials and objects, these sample scenarios (Figures 1B−D) demonstrate additional need for the developing new numerical techniques to characterize molecular dynamics within small compartments.

Despite the limitations of analytical models, autocorrelation curves generated under nonstandard conditions still contain valuable kinetic information. Computer simulations and numerical calculations with ideal detection volumes are sometimes used to

(21) Wirth, M.; Ludes, M.; Swinton, D. *Appl. Spectrosc.* **2001**, *55*, 663−669.
(22) Milon, S.; Hovius, R.; Vogel, H.; Wohland, T. *Chem. Phys.* **2003**, *288*, 171−186.
(23) Fradin, C.; Abu-Arish, A.; Granek, R.; Elbaum, M. *Biophys. J.* **2003**, *84*, 2005−2020.
(24) Lumma, D.; Keller, S.; Vilgis, T.; Radler, J. O. *Phys. Rev. Lett.* **2003**, *90*, 218301.
(25) Qian, H.; Elson, E. L. *Appl. Opt.* **1991**, *30*, 1185−1195.
(26) Hess, S. T.; Webb, W. W. *Biophys. J.* **2002**, *83*, 2300−2317.
(27) Hill, E. K.; de Mello, A. J. *Analyst* **2000**, *125*, 1033−1036.
(28) Enderlein, J.; Gregor, I.; Patra, D.; Fitter, J. *Curr. Pharm. Biotechnol.* **2004**, *5*, 155−161.
(29) Enderlein, J.; Gregor, I.; Patra, D; Dertinger, T.; Kaupp, U. B. *ChemPhysChem* **2005**, *6*, 2324−2336.
(30) Marrocco, M. *Appl. Opt.* **2004**, *43*, 5251−5262.
(31) Nishimura, G.; Kinjo, M. *Anal. Chem.* **2004**, *76*, 1963−1970.
(32) Hac, A. E.; Seeger, H. M.; Fidorra, M.; Heimburg, T. *Biophys. J.* **2005**, *88*, 317−333.
(33) Gennerich, A.; Schild, D. *Biophys. J.* **2000**, *79*, 3294−3306.
(34) Meng, F.; Ma, H. *J. Phys. Chem. B* **2005**, *109*, 5580−5585.

rationalize unexpected experimental trends or to determine approximate relationships between several variables in FCS measurements.[21,26,35,35–39] Applying the techniques of simulation-based fitting,[40] we describe a new method of numerically matching experimental data with synthetic autocorrelation curves to extract quantitative information.

Numerical fluorescence correlation spectroscopy (NFCS) mimics least-squares regression analysis by iteratively adjusting input parameters to minimize the residual differences between experimental data and synthetic curves generated by either simulation or direct calculation from an experimentally derived detection volume profile. We employ a distributed network of processors and a novel distributed autocorrelation algorithm to expedite this computationally intensive form of analysis. In order to demonstrate the effectiveness of the approach, we have analyzed a number of standard and nonstandard detection volume profiles to show that NFCS produces invariant results for the diffusion constant of Rhodamine B, despite large spatial aberrations in the detection volume. The numerical diffusion analysis demonstrated here has the potential to be expanded to a much wider array of FCS measurements that have been traditionally prohibited by a variety of nonstandard measurement conditions.

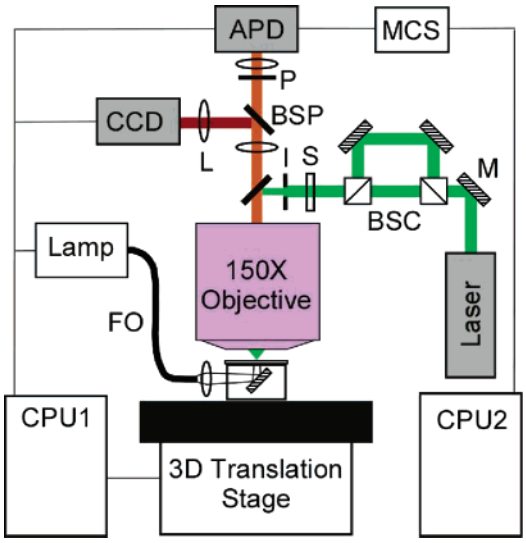

Figure 2. Schematic diagram of the scanning confocal laser microscope. APD, avalanche photodiode; BSC, nonpolarizing beam-splitting cube; BSP, beam-splitting plate; CCD, video camera; FO, fiber-optic bundle; I, iris; L, lens; M, mirror; MCS, multichannel scalar; P, pinhole; S, shutter.

EXPERIMENTAL SECTION

Apparatus. The confocal microscope (Figure 2) employs the chassis of an Axiotech Vario microscope (Carl Zeiss, Thornwood, NY) with a 150×, 1.25 NA epiplan-apochromat water immersion objective. The 543-nm line of an unpolarized 5-mW helium-neon laser (Melles Griot, Carlsbad, CA) is directed via mirrors through a nonpolarizing beam-splitting cube and is recombined with a second beam-splitting cube to create two distinct, nearly copropagating beam paths. Either beam can be selected for use in the microscope with a simple beam stop. Laser radiation passes through a computer-controlled shutter and an iris onto a dichroic mirror (555 DRLP, Omega Optical, Brattleboro, VT), which reflects the light to the back aperture of the objective. The light is focused to a sample resting on a 3D piezoelectric stage (17 AMD PZC, Melles Griot) that employs an active feedback-control loop. Fluorescence collected by the objective passes through an emission filter (590WB45, Omega Optical), after which half the light is sent to a video camera (CCD) and half is focused through a pinhole onto an avalanche photodiode single-photon counting module (SPCM-AQR-15, Perkin-Elmer, Fremont, CA). Power to the photodiode is supplied through a relay that is under computer control. Images from the video camera are captured with an IMAQ PCI 1409 card and Vision software (National Instruments, Austin, TX). Pulses from the photodiode are recorded by an MCS-Plus multichannel scalar card (EG&G Ortec, Oak Rdige, TN) and by pulse-counting circuitry onboard a multifunctional DAQ card (MIO-16E-1, National Instruments). An analog output board (PCI 6711, National Instruments) controls the piezoelectric stage motion, and the actual stage position is monitored using the analog-input channels on the MIO-16E-1. All software for monitoring and controlling the apparatus is written in LabVIEW 6.1 (National Instruments). The body of the microscope sits inside an acoustically damped enclosure that rests on a 4 ft. × 5 ft. × 12 in. optical bench with gimbal piston vibration isolators. Structural cross beams have also been added to the microscope to eliminate vibrations and reduce drift. The temperature and relative humidity in the laboratory remain constant to ±0.5 °C and ±2% during each measurement. Diffusion measurements are performed immediately following acquisition of the confocal detection volume map. To avoid photobleaching, the laser power is attenuated below 150 μW.

Detection Volume Maps. For measurements performed in a relatively homogeneous aqueous optical medium, accurate three-dimensional spatial profiles of the detection volume can be produced by scanning a small fluorescent sphere through the volume. A 20-μL suspension of 175-nm-diameter spheres (PS-Spec Fluospheres 540/560, Invitrogen Molecular Probes, Carlsbad, CA) is sonicated and applied to the surface of a silane-derivatized glass microscope slide (Silane-Prep slides, Sigma, St. Louis, MO). The slide surface is then rinsed after ~10 min. The carboxylated polystyrene beads adhere to the surface nonspecifically and are held in place in the aqueous immersion fluid during the scan without detectable movement. We also tested the acquisition of detection volume maps using smaller 43-nm-diameter fluorescent beads and found results comparable to the maps generated with the 175-nm spheres. We preferred to use the 175-nm beads because of their enhanced brightness and resistance to photobleaching. The size distribution of the 175-nm beads has a coefficient of variation of less than 3%, which helps ensure reproducibility of the maps. For an excitation power of ~20 nW,

(35) Dix, J. A.; Hom, E. F. Y.; Verkman, A. S. *J. Phys. Chem. B* **2006**, *110*, 1896–1906.
(36) Starchev, K.; Zhang, J.; Buffle, J. *J. Colloid Interface Sci.* **1998**, *203*, 189–196.
(37) Doose, S.; Tsay, J. M.; Pinaud, F.; Weiss, S. *Anal. Chem.* **2005**, *77*, 2235–2242.
(38) Martin-Brown, S. A.; Fu, Y.; Saroja, G.; Collinson, M. M.; Higgins, D. A. *Anal. Chem.* **2005**, *77*, 486–494.
(39) Wawrezinieck, L.; Rigneault, H.; Didier, M.; Lenne. P. *Biophys. J.* **2005**, *89*, 4029–4042.
(40) Nazarov, P. V.; Apanasovich, V. V.; Lutkovski, V. M.; Yatskou, M. M.; Koehorst, R. B. M.; Hemminga, M. A. *J. Chem. Inf. Comput. Sci.* **2004**, *44*, 568–574.

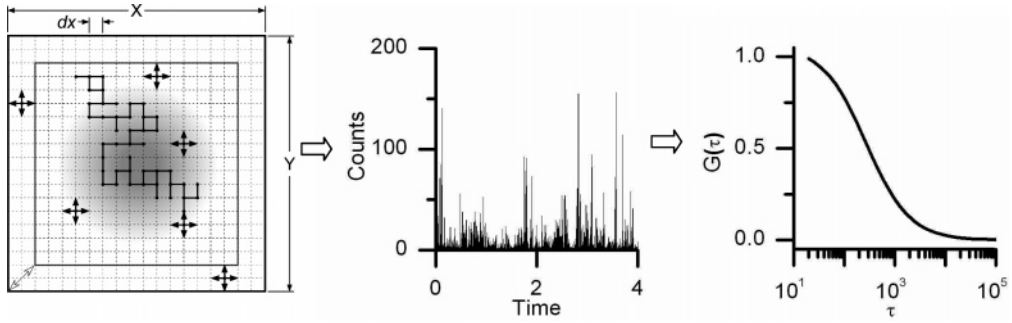

Figure 3. Schematic depiction of the SMDS. (A) The simulation divides space using a cubic lattice (only two dimensions are shown here). The step size dx is calculated from the diffusion constant D and the step time dt according to eq 4. The size of simulation space is calculated from the specified concentration for a given total number of molecules. The inner portion of simulated space contains the numerical map of the detection volume (shaded region). Typical map resolution is 15−75 nm. The proportion of inner and outer regions is not shown to scale. (B) A photon-burst record is generated as molecules randomly travel through the detection volume. (C) The SMDS contains a novel autocorrelation algorithm that enables the time records produced on separate processors in a distributed environment to be efficiently combined into a single autocorrelation curve, as if the data records from all of the processors were concatenated before correlation.

the maximum count rate produced during a scan is ~1000 counts/4 ms, with replicate trials on different beads producing ~15% RSD. Video inspection of spot circularity and the consistency of the maximum intensity suggest that single beads, as opposed to bead clusters, are used for mapping. Step sizes in the X and Y directions typically range from 30 to 40 nm, while the Z step size ranges from 100 to 350 nm, with a 10-ms wait time after each step. Maps represent rectangular volumes ranging in size from 1.5 μm × 1.5 μm × 5 μm to 3.5 μm × 3.5 μm × 14 μm in X, Y, and Z, respectively. After acquisition, a 10-pole 3D low-pass Butterworth filter is applied to the Fourier transform of the raw image, and the result is zero padded in the frequency domain to give an interpolated spatial profile with a resolution ranging from 15 to 75 nm, upon inverse transformation. The experimentally mapped confocal detection volume is then deconvolved from a spherical model of the probe bead using the Deconvolution J plug-in to the ImageJ software package.[41] After deconvolution, a user-defined threshold (typically 0.1−0.5% of the maximum intensity) is applied to remove background, and the map intensity is normalized to 1.

Single-Molecule Diffusion Simulator (SMDS). Simulations of molecular diffusion can produce synthetic autocorrelation curves for measurement scenarios with nonstandard FCS conditions. The SMDS passes simulation parameters (such as diffusion constant, molecular brightness, concentration, step size, collection bin width, and run time) into a simulator core, where the actual simulation takes place. For increased efficiency, the SMDS uses a modular core framework in which each core includes only the features necessary for a given type of simulation. For example, one core performs 2D simulations with fluorophore photobleaching while another excludes photobleaching calculations or enables a particular nanoscale geometric constraint. Each simulation uses the core with the smallest set of features necessary in order to maximize execution speed. The simulator performs a random walk on a 2D or 3D lattice with periodic boundaries (Figure 3). The total size of the simulated volume is calculated from the specified number of simulated particles and the particle concentration. Each diffusing species moves in simulation space on its own virtual lattice based on its characteristic diffusion coefficient, D, such that one step represents the root-mean-square displacement

$$\mathrm{d}x = \sqrt{2nD\ \mathrm{d}t} \tag{4}$$

where n is the number of dimensions of the lattice.[43] As long as the simulation step time, dt, is adequately small, this method produces results comparable to randomly distributed step sizes and significantly reduces the computation time by enabling integer, as opposed to floating point, arithmetic. Our results indicate that step times on the order of 500 ns are sufficient for open volume measurements, but smaller step times may be required for systems with very small geometric constraints.

The fluorescence signal is calculated from the position of the simulated molecules in the specified detection profile. The simulator uses either a numerical map of the detection volume or an analytical expression that describes the volume in the center of simulation space (Figure 3). For the analytical expression, if the particle falls within a user-specified threshold of the detection volume center during a given time step, the detected fluorescence intensity is calculated as

$$I_{3\mathrm{D}} = ae^{b(x^2+y^2)+cz^2}$$

$$b = -2/{\omega_1}^2$$

$$c = -2/{\omega_2}^2 \tag{5}$$

where a is an empirical value for the maximum photon detection efficiency per unit time for the given species. This parameter accounts for all of the photon losses in the system, including the molecular quantum yield, the collection solid angle of the microscope objective, reflection from optical surfaces, and the quantum efficiency of the APD. The values for a, b, and c are calculated before the simulation begins and are converted into simulation units: dx for spatial values and dt for temporal values.

(41) Rasband, W. S., http://rsb.info.nih.gov/ij, National Institutes of Health, Bethseda, MD, 1997−2006.

(42) Price, J. H.; Gough, D. A. *Cytometry* **1994**, *16*, 283−297.

(43) Berg, H. C. *Random walks in biology*; Princeton University Press: Princeton, NJ, 1993.

For both analytical and numerical spatial profiles, the detected emissions are summed over all particles and placed into collection time bins. To simulate shot noise, the final photon count for each bin is determined by randomly sampling from a Poisson distribution centered on the calculated photon sum for that bin. The simulated real-time intensity trace is then passed to postprocessing functions.

Direct Numerical Calculation. If an analyte obeys standard unconstrained Brownian dynamics, the autocorrelation function for a given diffusion coefficient can be calculated directly from numerical detection profile maps derived from either experimental measurement or standard analytical expressions.[26] Here, the autocorrelation function is understood as the spatial correlation of any two points in the detection profile multiplied by the probability that a particle moves from the first to the second point in a given lag time τ, integrated over all space. Thus, given Green's function for diffusion,

$$\Psi(\mathbf{r},\tau) = \frac{1}{(4\pi D\tau)^{3/2}} \exp\left(-\frac{|\mathbf{r}|^2}{4D\tau}\right) \qquad (6)$$

the autocorrelation function can be written as

$$G(\tau) = \int \int O(\mathbf{r}_1)\Psi(\mathbf{r}_1 - \mathbf{r}_2, \tau)O(\mathbf{r}_2)\, d\mathbf{r}_1\, d\mathbf{r}_2 \qquad (7)$$

where $O(\mathbf{r})$ is the map of the detection volume. For each τ, the double integral can be calculated efficiently from discrete data by multiplying each point in the map by the corresponding point in a convolution[44] of the map and diffusion profiles (O and Ψ), followed by a summation in three dimensions. The direct calculation of the autocorrelation function for a given diffusion constant and detection profile provides a fast alternative approach to simulation and can be used to corroborate the output of the SMDS when diffusive motion can be described analytically.

Distributed Processing Environment. To increase computational power and decrease execution time, we generate synthetic curves for NFCS analysis in a dynamic, heterogeneous, distributed computing environment using a simple custom message-passing system for internode communication. In this environment, a master computer sends work units to remote workstations and collates the results. Work units consist of small individual simulations, time segments from longer simulations, or the evaluation of eq 7 at a given time delay. The remote processors run at a low priority, allowing computation to proceed on workstations without disturbing other users. Additionally, the SMDS benefits from a load-balancing procedure to maximize performance across a diverse network and can thus accommodate both dedicated scientific computing networks and collections of laboratory workstations available in most academic settings.

The SMDS programming environment presents a unified interface to all of the diverse simulator cores in the form of a module in the Python programming language. Computationally intensive routines (the simulator cores and matrix manipulation routines) are coded in C for speed. Simulations are performed

(44) Press, W. H.; Teukolsky, S. A.; Vetterling, W. T.; Flannery, B. P. *Numerical recipes in C: The art of scientific computing*; Cambridge University Press: Cambridge, 1992.

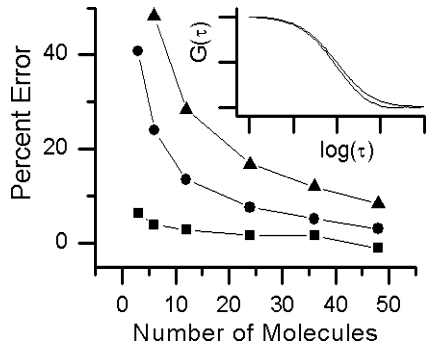

Figure 4. Error in the diffusion constant (eq 3) arising from a fit of simulated data using the standard detection profile (eq 2). Each point represents the average of 20 simulations lasting for 100 s with $D = 1.0 \times 10^{-7}$ cm^2/s. (■) 0.1 μm^{-3} (170 pM); (●) 1.0 μm^{-3} (1.7 nM); (▲) 2.5 μm^{-3} (4.2 nM). The general increase in error as a function of concentration results from non-Poissonian conditions due to an insufficient total number of molecules for the stated concentration. Inset: Comparison of autocorrelation functions obtained from simulations of equivalent concentration run with 5 molecules (left curve) and 500 molecules (right curve). The non-Poissonian conditions caused by too few simulated molecules shorten the average fluorescence burst width and attenuate the trailing portion of the autocorrelation curve.

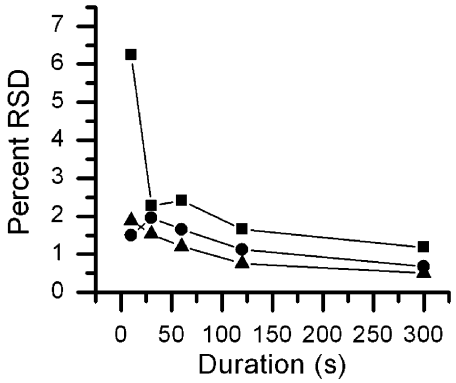

Figure 5. Precision of the diffusion constant (eq 3) arising from a fit of simulated data using the standard detection profile (eq 2) as a function of equivalent real-time duration and concentration. Each point represents 10 simulations with 50 molecules and $D = 4.0 \times 10^{-6}$ cm^2/s. (■) 0.1 (170 pM), (●) 0.5 (830 pM), and (▲) 1.0 μm^{-3} (1.7 nM).

in batch with an XML-formatted input/output file that encapsulates the simulation conditions, processed data, and run-time information. The Python interface allows quick and easy implementation of complex experimental and data processing procedures.

Distributed Multi-τ Autocorrelator. When generating synthetic curves via simulation, computational throughput can be limited by network I/O speeds if lengthy fluorescence intensity records must be transferred from remote processors to the master computer. NFCS requires only the autocorrelation of the real-time fluorescence trace, alleviating the need to manipulate and store the entire time record. However, existing correlation routines require temporary access to the continuous stream of simulated real-time data. In a distributed processing environment, these data would still have to be transferred across the network. To alleviate the data-transfer burden, we have developed a new distributed autocorrelation algorithm that begins the correlation on-line at the remote source of the data.[45] The master computer then collates

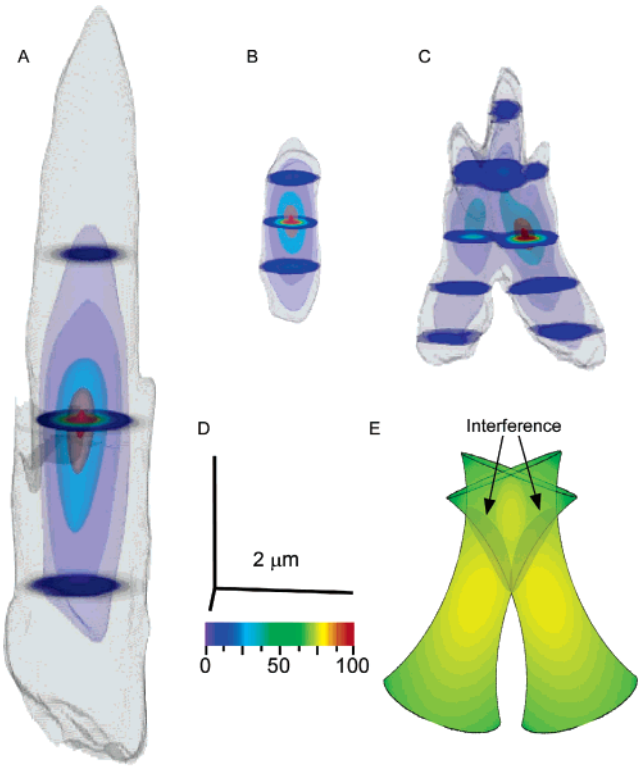

Figure 6. Detection volume maps resulting from differing optical conditions. The isosurfaces indicate different detection efficiency levels and range from 0.5% (outermost surface) to 95% (innermost surface) with cross-sectional slices to aid 3D visualization. Each map has been interpolated to a resolution of 15−75 nm. (A) 400-μm pinhole, single beam, underfilled objective. (B) 75-μm pinhole, single beam, overfilled objective. (C) 200-μm pinhole, crossed double beam, overfilled objective. (D) Scale and intensity range for maps. (E) Depiction of the crossed double beam detection volume and the regions of interference that give rise to the complex spatial structure seen in (C).

a dramatically reduced set of data from each remote processor to compute the final autocorrelation curve.

Matching Experimental Data. Although it is difficult or impossible to generate analytical models for many FCS measurement scenarios, some scenarios can be modeled numerically quite easily. NFCS extracts kinetic information from experimental data by comparing the experimental autocorrelation curve with a synthetic autocorrelation curve that is based on a guess for the input parameters. The guess is then iteratively adjusted to minimize the difference between the two curves. We employ the Simplex minimization algorithm[46,47] to perform the parameter optimization. Noise in the merit function due to random variations in simulation output inhibits the Simplex algorithm from locating the global minimum; thus, Simplex minimization is used only to estimate the optimal parameters for simulations. The global minimum is then established by fitting several evaluations of the merit function near the estimate with a quadratic equation. We typically fit 25 points spanning ±5% of the estimated optimal parameter. NFCS based on direct calculations of the autocorrelation function can rely on the results of the Simplex minimization directly since the calculation is not subject to random variation.

RESULTS AND DISCUSSION

Simulator Accuracy and Precision. The number of molecules simulated has the greatest effect on the simulation's accuracy. Even at so-called single-molecule concentrations, there remains a small but measurable probability of finding multiple fluorophores in the detection volume at the same time. Each multiple-occupancy event yields a fluorescence burst that lasts much longer than a burst from a single-molecule crossing since individual crossing events are combined into a single, elongated burst. Multiple occupancies thus lengthen the average fluorescence burst and widen the contour of the resulting autocorrelation function.

Under actual experimental conditions, the number of diffusing fluorophores is very large, and the number of molecules in the detection volume can be approximated by Poisson statistics:[43]

$$P(m) = \frac{\langle N \rangle^m}{m!} e^{-\langle N \rangle} \tag{8}$$

where $P(m)$ is the probability of finding m molecules in the detection volume if the average number of molecules in the detection volume is $\langle N \rangle$. Thus, in a 1-nM solution, a 10^{-15}-L volume should contain one molecule 33% of the time and two molecules 9.93% of the time, or 993 ms out of a 10-s experiment. However, the number of molecules in the simulation is always much smaller than the number in a real solution; thus, the number of molecules in the simulated detection volume follows a binomial distribution:[43]

$$P_n(m) = \binom{n}{m}\left[\frac{\langle N \rangle}{n}\right]^m\left[1 - \frac{\langle N \rangle}{n}\right]^{n-m}$$

$$\binom{n}{m} \equiv \frac{n!}{m!(n-m)!} \tag{9}$$

where $P_n(m)$ is the probability of finding m out of n simulated molecules in the detection volume. In a 1-nM simulation with only five molecules, two molecules share the detection volume only 9.87% of the time, or 987 ms out of a 10-s simulation, leaving 6 ms in which a dual occupancy should have been simulated but was not. These 6 ms represent fluorescence bursts that should have been conjoined. In their absence, the average fluorescence burst width is artificially short, which is reflected in the latter portion of the correlation function (Figure 4, inset). The effect on the calculated value of D depends on the detection-volume crossing time. For detection-volume crossing times on the order of 0.1 ms, the discrepancy introduces an error of 30% in the resulting calculated D. As concentration increases, the number of simulated molecules must increase to maintain accuracy (Figure 4). But, since the computation time increases with the number of molecules, a tradeoff exists between simulating large concentrations with little error and the length of time needed to perform the calculation. For detection volumes on the order of 0.1 fL, reasonable results (within 10%) can be obtained with 10−20 molecules for concentrations less than 1.5 nM, while good results (within 5%) can usually be obtained with 30−40 molecules.

(45) Culbertson, M. J.; Burden D. L. *Rev. Sci. Instrum.* In press.
(46) Nelder, J. A.; Mead, R. *Comput. J.* **1965**, *7*, 308−313.
(47) Yarbro, L. A.; Deming, S. N. *Anal. Chim. Acta* **1974**, *73*, 391−398.

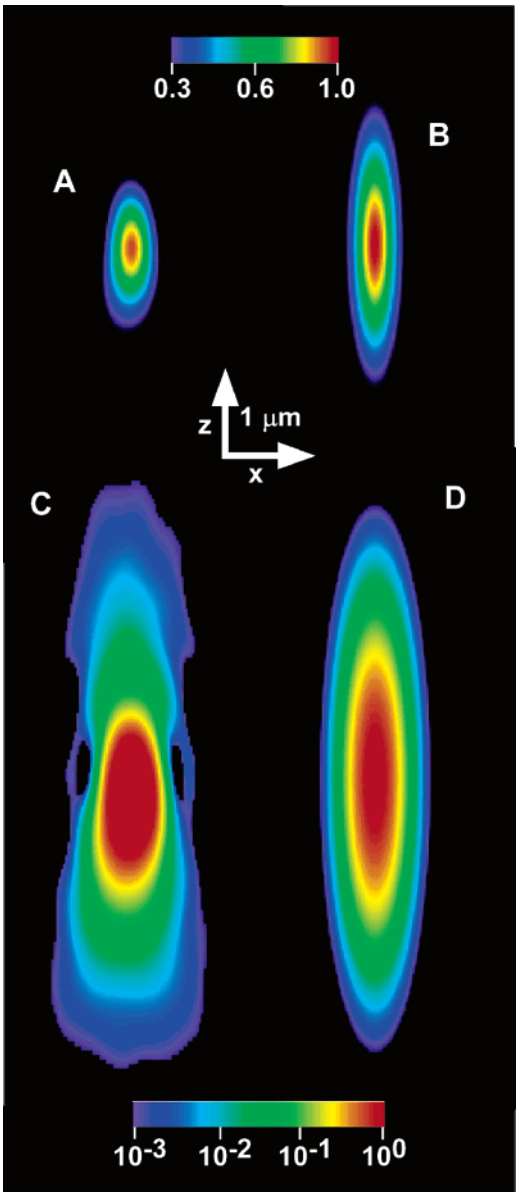

Figure 7. Cross section of a 0.344-fL detection-volume map acquired using a 150-μm pinhole with an overfilled objective (A and C, linear and logarithmic scales, respectively) and the closest corresponding Gaussian model of three local minimums obtained in fitting the autocorrelation curve with the standard 3D FCS equation (eq 3). The value for D used in calibration was obtained by NFCS analysis, and the parameters ω_1 and ω_2 were allowed to vary independently (B and D). Since the Gaussian model (0.448 fL) cannot represent the Airy rings seen in the midsection of (C) or follow the expanding contour at high and low Z, the approximation assumed by the standard FCS equation misrepresents the actual volume by ~30%.

Achieving less than 1% error requires over 200 simulated molecules. Larger detection volumes require more molecules for a comparable level of accuracy.

As would be expected, the precision in the extracted values for the diffusion coefficient improves as the concentration and simulation duration increase, since both of these factors yield a more thorough sampling of all possible paths through the detection volume (Figure 5). As with accuracy, a tradeoff exists between high precision and the length of time required for simulation. But, in many detection volumes, reasonable precision

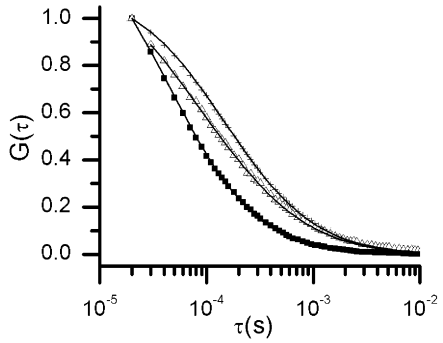

Figure 8. Autocorrelation functions produced using numerical maps A (+), B (■), and C (Δ) from Figure 6 and the matched synthetic curves from NFCS analysis (line). Curves were collected for 300 s with a solution of ~1.7 nM Rhodamine B. The baseline has been subtracted, and the curves have been normalized such that the first point equals 1.

(6%) is possible even for short (10 s), low-concentration (150 pM) simulations.

Simulator Speed. NFCS computations run primarily on a bank of 25 3.0-GHz Pentium 4 processors using NetBSD 3.0, along with several other GNU/Linux and Microsoft Windows computers. Because the distributed system is dynamic, processors can be added or dropped during a calculation as need arises. Simulation run time depends on the simulation parameters, primarily the simulation core chosen, the number of molecules simulated, the duration of simulated time, and concentration. A typical 60-s simulation of 40 molecules at 166 pM takes ~178 s on a single 3.0-GHz NetBSD workstation. This run time decreases to ~23 s when eight workstations work together, just over one-eighth the uniprocessor time. For large detection volumes, we found that 300-s simulations with 250−1000 molecules were necessary for the desired precision in NFCS results. These more-intensive simulations can take 10−15 min each when distributed over ~20 processors. The Simplex minimization frequently requires 20−30 evaluations of the autocorrelation function, which thus takes 4−6 h. Since NFCS analysis via simulation requires an additional set of ~25 evaluations in the region of the minimum, the total analysis time can be as much as 12 h. On a single processor, the calculations would run continuously for 12 days.

Detection Volume Images. To test the effectiveness of NFCS, we performed diffusion measurements of Rhodamine B using a variety of optical configurations, including some that deviated extensively from the standard model (Figure 6). We used different combinations of pinhole size and filling of the objective back aperture to alter the geometry (Figure 6A,B,7). For demonstration purposes, we also created a highly irregular detection volume using two slightly misaligned laser beams (Figure 6C). Near the focal plane of the objective, the two beams cross to form a profile with varied structure, which is due in part to laser interference (Figure 6E). Detection volume maps and their corresponding autocorrelation data were collected under six different optical configurations: (1) single beam, 150-μm pinhole, underfilled objective; (2) single beam, 150-μm pinhole, overfilled objective; (3) single beam, 400-μm pinhole, underfilled objective; (4) single beam, 75-μm pinhole, overfilled objective; (5) skewed single beam, 150-μm pinhole, overfilled objective, (6) double beam, 200-μm pinhole, overfilled objective. The resulting size and shape of the

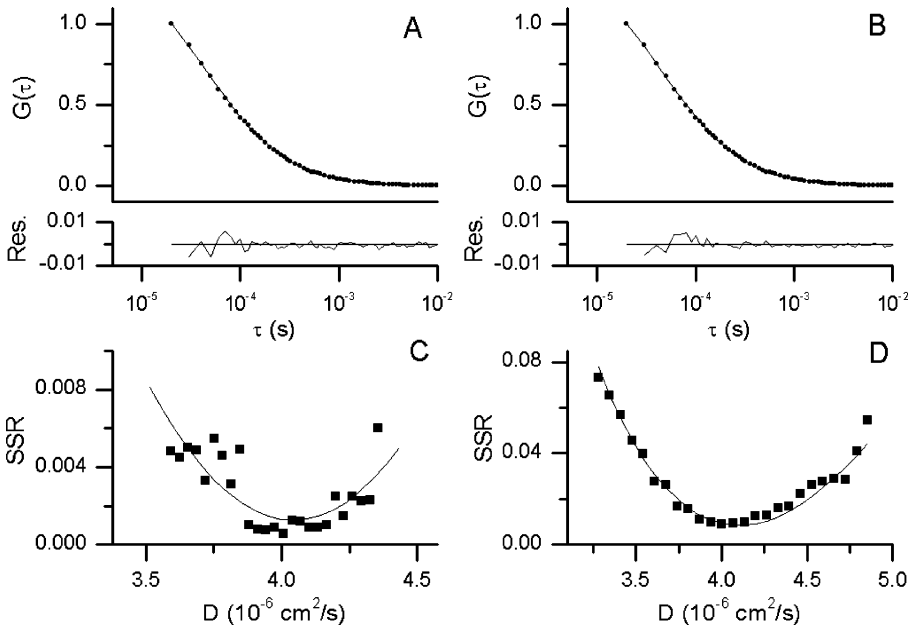

Figure 9. (A) Experimentally acquired autocorrelation function (●, 300-s integration) matched by iteratively adjusting the simulated diffusion constant (– best matched result, $D = 3.99 \times 10^{-6}$ cm^2/s). (B) The same experimental autocorrelation function (●) matched via direct calculation (– best matched result, $D = 4.03 \times 10^{-6}$ cm^2/s). (C) Matching via simulation involves calculating the sum of squared residuals (SSR) between simulated and experimental curves in a region around an estimate of D and fitting with a parabola. (D) Autocorrelation functions generated via simulation (points) and direct calculation (line) agree closely over a range of diffusion constants.

Table 1. Rhodamine B Diffusion Constants Determined by NFCS Using Either Simulation or Direct Calculation[a]

	simulation (cm^2/s)	direct calc (cm^2/s)
150-μm pin., underfilled	$(4.21 \pm 0.01) \times 10^{-6}$	$(4.37 \pm 0.01) \times 10^{-6}$
150-μm pin., overfilled	$(4.34 \pm 0.07) \times 10^{-6}$	$(4.47 \pm 0.01) \times 10^{-6}$
400-μm pin., underfilled	$(4.16 \pm 0.05) \times 10^{-6}$	$(4.22 \pm 0.02) \times 10^{-6}$
75-μm pin., overfilled	$(3.97 \pm 0.16) \times 10^{-6}$	$(4.00 \pm 0.17) \times 10^{-6}$
150-μm pin., skewed	$(4.24 \pm 0.04) \times 10^{-6}$	$(4.36 \pm 0.04) \times 10^{-6}$
200-μm pin., crossed beams	$(4.32 \pm 0.1) \times 10^{-6}$	$(4.37 \pm 0.08) \times 10^{-6}$
average	$(4.21 \pm 0.04) \times 10^{-6}$	$(4.30 \pm 0.05) \times 10^{-6}$

[a] Averages and standard errors are for three trials of each measurement scenario.

3D profiles generally agree with theoretical predictions[26] and readily show deviations from an ideal Gaussian (Figures 6 and 7). Three images were acquired for each configuration using separate 175-nm beads. The detection volume sizes after processing ranged from 0.12 μm^3 for a 75-μm pinhole to 1.2 μm^3 for a 400 μm-pinhole arrangement. Generally, configurations that produce larger optical volumes result in longer average molecular crossing times and shift the corresponding autocorrelation curve to larger values of τ. However, the specific 3D shape of the profile also gives rise to a distinct curve contour, which can demonstrate the presence of nonideal optical conditions (Figure 8).

To obtain the radial and axial dimensions of the detection volume for FCS analysis, experimentalists typically fit the autocorrelation curve produced by a known diffusion standard with eq 3 in a calibration step. However, deviations in the volume profile from the Gaussian model can cause multiple minimums in the calibration fit, sometimes with highly unrealistic values (such as $\omega_1 = 445$ nm and $\omega_2 = 21\,867$ nm for the dramatically distorted volume of Figure 6C) due to the lack of correspondence between actual and assumed Gaussian contours. Even when the likeliest result is used, the size of the Gaussian model may not accurately reflect the actual detection volume size due to unmatched spatial features (Figure 7). This difference between the actual detection volume size and the size of the calibrated Gaussian model can lead to poor absolute concentration measurements in FCS analysis. Despite the difference in volume size, calibrated fits using Gaussian-shaped profiles can produce residual trends similar to NFCS for many common measurement scenarios, if ω_1 and ω_2 are allowed to vary independently during calibration. Holding the axial-to-radial ratio constant, however, as is common practice in FCS analysis, frequently results in systematic residual differences between experimental curves and FCS fits, since the parameters have less freedom to accommodate the non-Gaussian features of the detection volume. When deviations in the detection profile are minor and the axial ratio is not held constant, the error in D established by traditional FCS fits is <5%. However, as the deviations increase (e.g., Figure 6C), the error can grow to over 40%, and systematic residuals may encourage the inappropriate substitution of more complex analytical models.

Diffusion Analysis. For NFCS analysis via simulation, the SMDS must be given a rough estimate of the concentration and apparent brightness of diffusing molecules. The concentration estimate can be derived from the experimental autocorrelation function, which contains information about the average number of molecules in the detection volume:[20]

$$G(0) = \gamma/\langle N \rangle + 1 \tag{10}$$

where $\langle N \rangle$ is the time-averaged number of fluorescent particles in the detection volume. The constant γ describes the shape of the detection volume and is given by

$$\gamma = w_2/w_1$$

$$w_n = \int \left[\frac{O(\mathbf{r})}{O(0)}\right]^n \mathrm{d}\mathbf{r} \tag{11}$$

where $O(\mathbf{r})$ is the collected intensity profile of the detection volume. The concentration is thus

$$\langle C\rangle = \langle N\rangle/w_1 \tag{12}$$

Finally, the effective maximum molecular fluorescence can be determined from the average detected intensity in the experimental real-time record:[48]

$$\langle I\rangle = I_0\langle N\rangle \tag{13}$$

Since the calculated value of $G(0)$ from experimental data is always inflated due to shot noise, $G(0)$ is estimated from data at small delay times.[1] Concentration and intensity estimates are not required for NFCS analysis via direct calculation. All experimental and synthetic autocorrelation curves were prepared for comparison by subtracting the baseline and normalizing the smallest delay time to a value of 1.

For each detection profile map, a sample of ~1.7 nM Rhodamine B solution was placed in a small container under the objective and a 300-s record of real-time fluorescence data was collected and autocorrelated. The experimental autocorrelation function was processed using NFCS analysis with both simulated and calculated synthetic curves to extract diffusion information, and the results of the three trials for each optical configuration were averaged. Simulations used at least 250 molecules. Simulation and direct calculation produce very similar curves over a wide range of diffusion constants (Figure 9D), and NFCS analysis via simulation and calculation differed by less than 4% in most cases. In all cases, the residual values were small, even for detection volumes with nonstandard profiles (Figures 8 and 9). The averages of the matched diffusion constants for each measurement scenario ranged from $(3.67-4.67) \times 10^{-6}$ cm^2/s with an overall average of $(4.25 \pm 0.05) \times 10^{-6}$ cm^2/s (Table 1). The means for different optical configurations were statistically indistinguishable ($\alpha = 0.01$), despite significant differences in the detection volume profiles, and the averages fall within the range of reported diffusion constants for Rhodamine B.[49−52]

CONCLUSION

We described a new method for the analysis of molecular dynamics that is based on traditional fluorescence correlation spectroscopy, but circumvents many of its inherent limitations by numerically generating correlation curves from an experimentally determined map of the detection volume profile. As a demonstration of this new approach, we showed that simple diffusion measurements via NFCS remain invariant, regardless of the distortions present in the optical detection volume. Results were consistent whether synthetic curves were obtained via simulation or direct calculation. Direct calculation of the autocorrelation function is generally faster than simulation and less prone to random variation, but simulation allows greater freedom to model a variety of scenarios that cannot be described analytically. In contrast with NFCS, fitting experimental data with FCS expressions calibrated using a fixed axial ratio can result in systematic residuals. Even if the radial and axial parameters are allowed to vary independently during calibration, the inability of the standard model to match the particular features of the actual detection volume can lead to an inaccurate representation of the volume's shape and size. We believe that NFCS will be generally applicable whenever experimental conditions deviate from the assumptions of traditional FCS, including measurements that involve nanoscale geometric constraints. Thus, we anticipate that the numerical concepts described here will be relevant to both one- and two-photon correlation measurements and will broaden the possibilities for molecular dynamics analyses in many new and interesting systems.

ACKNOWLEDGMENT

Partial funding for this work was provided by the Henry Dreyfus Teacher−Scholar Awards Program, Research Corporation, the donors of the Petroleum Research Fund, administered by the American Chemical Society, the Wheaton College Alumni Association, and the National Science Foundation (0550005). J.J.K. thanks the NIST Office of Law Enforcement Standards. John C. Hayward and Cary G. Gray of the Wheaton College Math and Computer Science Department, and Brian Hurley of the Wheaton College Institutional Research and Assessment Department also provided critical computer support for this work.

Received for review October 27, 2006. Accepted March 18, 2007.

AC062013M

(48) Müller, J. D.; Chen, Y.; Gratton, E. *Methods Enzymol.* **2003**, *361*, 69−92.
(49) Culbertson, C. T.; Jacobson, S. C.; Ramsey, J. M. *Anal. Chem.* **1998**, *70*, 3781−3789.
(50) Rani, S. A.; Pitts, B.; Stewart, P. S. *Antimicrob. Agents Chemother.* **2005**, *49*, 728−732.
(51) Ramsey, J. D.; Jacobson, S. C.; Culbertson, C. T.; Ramsey, J. M. *Anal. Chem.* **2003**, *75*, 3758−3764.
(52) Sera, Y.; Matsubara, N.; Otsuka, K.; Terabe, S. *Electrophoresis* **2001**, *22*, 3509−3513.